applied sciences

MDPI

Article

Mechanochemical Synthesis of the Catechol-Theophylline Cocrystal: Spectroscopic Characterization and Molecular Structure

Juan Saulo González-González [1,*], Raquel Jiménez-López [1], David Ortegón-Reyna [2], Gabino Gonzalez-Carrillo [3] and Francisco Javier Martínez-Martínez [4]

[1] Instituto de Farmacobiología, Universidad de la Cañada, Carretera Teotitlán-San Antonio Nanahuatipan km 1.7 s/n, Teotitlán de Flores Magón, Oaxaca C.P. 68540, Mexico; raquel_jmz21@hotmail.com
[2] Centro Multidisciplinario de Investigación Científica, Calle Heliodoro Garcia No. 36, Colonia Arcoiris, Manzanillo, Colima C.P. 28219, Mexico; dortegon@cemic.mx
[3] Tecnológico Nacional de México, Instituto Tecnológico Jose Mario Molina Pasquel y Henriquez, Unidad Académica Tamazula, Carretera Tamazula-Santa Rosa 329, Tamazula de Gordiano, Jalisco C.P. 49650, Mexico; gabino.gonzalez@tamazula.tecmm.edu.mx
[4] Facultad de Ciencias Químicas, Universidad de Colima, km 9 Carretera Colima-Coquimatlán, Coquimatlán, Colima C.P. 28400, Mexico; fjmartin@ucol.mx
* Correspondence: juan_saulo@unca.edu.mx

Citation: González-González, J.S.; Jiménez-López, R.; Ortegón-Reyna, D.; Gonzalez-Carrillo, G.; Martínez-Martínez, F.J. Mechanochemical Synthesis of the Catechol-Theophylline Cocrystal: Spectroscopic Characterization and Molecular Structure. *Appl. Sci.* **2021**, *11*, 3810. https://doi.org/10.3390/app11093810

Academic Editor: Snezana Agatonovic-Kustrin

Received: 25 March 2021
Accepted: 12 April 2021
Published: 23 April 2021

Featured Application: ATR-IR spectroscopy allowed to determine the modification of the solid form of theophylline.

Abstract: Pharmaceutical cocrystallization offers the possibility to modify the physicochemical and biopharmaceutical properties of active pharmaceutical ingredients. The mechanochemical synthesis and spectroscopic characterization of the catechol-theophylline (CAT-TEO) cocrystal is reported. The cocrystal was prepared by the solvent-assisted grinding method. The ATR-IR spectroscopy study allowed to determine the formation of the cocrystal because the O-H and C=O stretching bands in the CAT-TEO cocrystal were shifted with respect to the starting materials, suggesting the formation of the C=O···H-O hydrogen bond interaction. Infrared spectroscopy also allowed to discard hydration of the cocrystal, and polymorphic transitions of the starting products as a consequence of the mechanochemical grinding. The X-ray powder diffraction and thermal studies confirmed the formation of a new solid phase. In the solid state ^{13}C NMR spectra of the cocrystal, the signals were shifted with respect to the starting products. The ^{13}C NMR chemical shifts of the CAT-TEO cocrystal were simulated by using the gauge including the atomic orbital (GIAO) method. These results showed a good correlation between the experimental and calculated ^{13}C NMR results. Theoretical calculations and natural bonding orbital analysis (NBO) at a B3LYP/6-31G(d,p) level of theory were performed to obtain structural information of the cocrystal.

Keywords: cocrystal; theophylline; catechol; IR spectroscopy; theoretical calculations

1. Introduction

Theophylline is a methyl-xanthine drug that occurs naturally in products such as coffee, tea and cocoa nuts, and is used for the treatment of asthma and chronic obstructive pulmonary disease [1]. Molecular recognition of theophylline has been exploited in solution and a solid state. In solution, it has led to the development of molecular receptors [2,3]; meanwhile, in solid state, it has been applied in the design and synthesis of pharmaceutical cocrystals. Pharmaceutical cocrystals are multi-component crystalline solids formed by a pharmaceutical active ingredient (API) and a cocrystal former, stabilized by noncovalent interactions, principally hydrogen bonds [4].

Theophylline is a model molecule [5] for cocrystallization studies because bears in their chemical structure carbonyl groups are able to act as hydrogen bond acceptors (theophylline can also act as a donor because it has a N-H group), allowing the formation of cocrystals with different cocrystal coformers, such as: organic acids, diclofenac, nicotinamide, acesulfame, to mention some [6–9].

On the other hand, catechol or 1,2-dihydroxybenzene contain hydroxyl groups, which can act as hydrogen bond donors for the synthesis of cocrystals due to their ability to form O-H···X (X = O, N) hydrogen bonds, with the advantage that they form neutral hydrogen bonds, discarding the formation of salts. Some examples of API's that have formed cocrystals with catechol are nalidixic acid, tenoxicam, brexpiprazole, and isoniazid [10–13].

From the reported cocrystallization methods, the most used are the solvent evaporation method and the solvent-assisted grinding method [14]. In the solvent evaporation method, the API and the cocrystal former are dissolved in a suitable solvent, which is left to evaporate to obtain the cocrystal. This method is used to obtain suitable monocrystals for single crystal X-ray diffraction; however, it depends on the solubility of the compounds, it is necessary to wait a few days for the evaporation of the solvent, and the presence of the solvent can lead to the formation of solvates. On the other hand, in the solvent-assisted method, the API and the cocrystal former are ground together with some solvent drops. The mechanochemical energy favors the rearrangement of the molecules in solid state to form the cocrystal. This method offers the advantage of reproducibility, rapid screening and independence of the solubility of the starting products [14].

Solid-state monitoring techniques such as powder and single X-ray diffraction, solid-state nuclear magnetic resonance (NMR) and infrared spectroscopy (IR) are employed in the characterization of pharmaceutical cocrystals [15]. IR spectroscopy has been used to determine the formation of cocrystals, polymorphs, salts and solvates [16–18]. Attenuated total reflection (ATR) IR spectroscopy offers the advantage of rapid determination (the sample does not need previous preparation for the analysis) of the formation of the new solid between the API and the cocrystal former by the shift of the IR absorption bands of the functional groups in the cocrystal with respect to the starting components [19,20]. Solid state nuclear magnetic resonance is used for the characterization of pharmaceutical cocrystals and polymorphs because it gives structural and crystallographic information and is sensitive to hydrogen bonding [21,22].

In order to exploit the ability of the dihydroxybenzenes to form O-H···O=C hydrogen bond interactions with theophylline, here we report the mechanochemical synthesis of the catechol-theophylline cocrystal (CAT-TEO) (Figure 1) obtained by the solvent-assisted grinding method. The ATR-IR spectroscopy has played an important role because it allowed to rapidly determine the formation of the powder cocrystal, discarding the hydrate formation. The characterization of the CAT-TEO cocrystal was completed using solid-state ^{13}C NMR, powder X-ray diffraction and DSC calorimetry. The molecular structure of the CAT-TEO cocrystal was obtained by theoretical calculations.

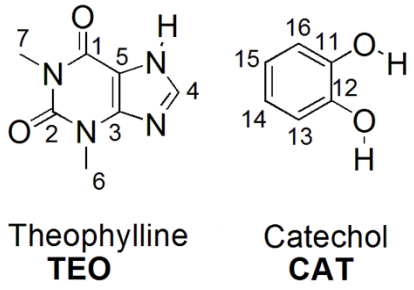

Figure 1. Chemical structure and numbering of CAT and TEO.

2. Materials and Methods

2.1. Mechanochemical Synthesis

Theophylline anhydrous, catechol and dichloromethane were purchased from Aldrich. All the compounds were used as received.

The CAT-TEO cocrystal was prepared by grinding 0.486 g of anhydrous theophylline (2.72 mmol) with 0.300 g of catechol (2.7 mmol) in a pestle with a mortar for 15 min. Before the start of grinding, 0.5 mL of dichloromethane was added; then, the mixture was ground for 3 min. After grinding, the powder was collected in the center of the mortar. After that, 0.5 mL of dichloromethane was added to the powder mixture and ground for an additional 3 min. The cycle of adding 0.5 mL of dichloromethane and grinding for 3 min was repeated five times until 15 min of grinding was completed. The powder obtained was stored in a glass vial.

In order to discard polymorphic transitions as a consequence of the grinding, the starting products were ground individually (2.72 mmol) with dichloromethane under the same conditions of the CAT-TEO mixture.

To evaluate the water absorption effect over the catechol and theophylline, 2.72 mmol of each starting product were ground with 0.5 mL of water for 15 min. Water was added before the start of grinding. The 1:1 mixture of CAT-TEO was treated in the same way.

All the attempts to obtain single crystals for diffraction were unsuccessful.

2.2. Instruments

Infrared spectra of solid samples of the API´s, the crystal formers and the ground products were obtained neat in a Bruker Tensor-27 spectrophotometer (16 scans, spectral range 600 to 4000 cm^{-1}, resolution 4 cm^{-1}) equipped with an attenuated total reflection (ATR) system. IR spectra were acquired and processed using the OPUS software version 7.2 (Bruker Optik GmbH).

X-ray powder diffraction data were collected on a PAN Analytical X-Pert PRO diffractometer with CuKα1 radiation (λ = 1.5405 Å, 45 kV, 40 mA) from 2.02 to 49.93° in 2θ.

Solid-state 13C NMR spectra were recorded on a Bruker 400 Avance III (^{13}C, 100 MHz) instrument with a Cross Polarization Magic/Angle Spinning (CP/MAS) unit at 25 °C. The spinning rate and acquisition time were 8 kHz and 32 msec. A 4-mm bullet-type Kel-F zirconia rotor contained about 100 mg of sample. The recycle time of the pulse was 3 s. The signal of the adamantane was used as external reference (δ = 38.48 ppm).

Differential scanning calorimetry was performed on a TA Instruments Q2000 DSC. Temperature calibration was performed using an indium standard. Three milligrams of the sample were placed in an aluminum pan with a gradient of 5.00 °C /min from 50 °C to 200 °C. Thermal gravimetric analysis was performed using a TA instruments Q5000IR analyzer. The samples were loaded in an aluminum pan. The samples were heated at the rate of 5.00 °C/min, under nitrogen.

2.3. Theoretical Calculations

Two optimized geometries models as CAT-TEO_1 and CAT-TEO_2 were performed using the density functional theory (DFT) calculations, with the B3LYP hybrid functional and the 6-31G(d,p) basis set, using the Gaussian 09 software [23]. Vibrational frequencies were calculated to ensure that the optimized geometries correspond to local minima on the potential energy surface. Natural bond orbital (NBO) Fock matrix analysis at the same level of theory was performed to elucidate the electron density distribution within the molecules of the complexes, while ^{13}C NMR chemical shifts and magnetic shieldings were simulated using the gauge including atomic orbital (GIAO) method at B3LYP/6-31G(d,p) and referenced with the TMS HF/6-31G(d) option of the GaussView software [23].

3. Results and Discussion

3.1. IR Spectroscopy

ATR-IR spectroscopy study was performed to determine the formation of the new crystalline solid-phase solid by monitoring the shifts of the hydroxyl (O-H), and carbonyl (C=O) stretching frequencies in the CAT-TEO (Figure 2) ground solid with respect to the starting products (CAT and TEO, Figure 2). The IR spectra were acquired directly after the CAT-TEO ground process, and from the bulk CAT and TEO. TEO and CAT were ground in cycles of 3 min, until a total of 15 min of grinding time. IR spectra of CAT and TEO were assigned according to previous reports [16,18].

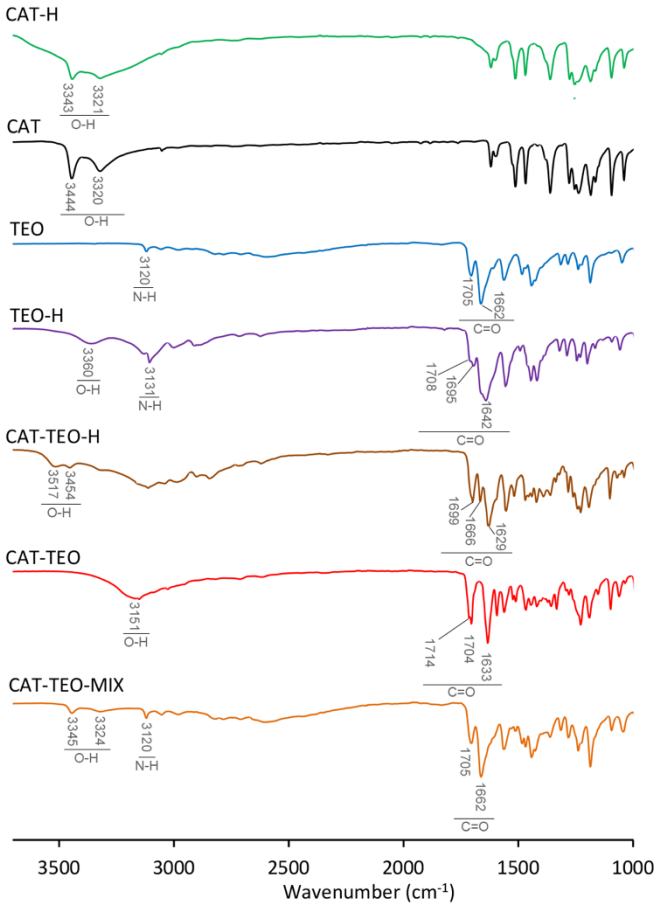

Figure 2. IR spectra of CAT-H (catechol ground with water), CAT (catechol), TEO (theophylline), TEO-H (theophylline ground with water), CAT-TEO-H (catechol and theophylline ground with water), CAT-TEO (catechol and theophylline ground with dichloromethane), and CAT-TEO-MIX (physical mixture of catechol and theophylline).

In the IR spectrum of CAT-TEO obtained after 15 min of grinding (Figure 2), the O-H stretching bands (Table 1) were shifted with respect to the starting products and the physical mixture (CAT-TEO-MIX, Figure 2). This suggests the formation of a C=O···H-O hydrogen bond between CAT and TEO. The free form of CAT showed two O-H stretching bands (Figure 2)—one in the 3500 to 3400 cm^{-1} range and the other in the 3300 cm^{-1} range of the phenolic O-H stretching frequency. As a consequence of the rearrangement in the intermolecular hydrogen bonding pattern from O-H···O-H in the free form to the O-H···O=C in the cocrystal, the band in the 3500 to 3400 cm^{-1} range was shifted to lower frequencies with $\Delta(\nu O\text{-}H) = -293$ cm^{-1}. Meanwhile, the band in the 3300 cm^{-1} range shifted to higher frequencies with $\Delta(\nu O\text{-}H) = 105$ cm^{-1}. This shift is in agreement with previous reports about molecular complexes formed by O-H···O=C hydrogen bond interactions between catechol with oxalamates and carbamates [24,25].

Table 1. O-H, C=O and N-H stretching frequencies (cm^{-1}) CAT-H (catechol ground with water), CAT (catechol), TEO (theophylline), TEO-H (theophylline ground with water), CAT-TEO-H (catechol and theophylline ground with water), CAT-TEO (catechol ground with dichloromethane), CAT-TEO-MIX (physical mixture of catechol and theophylline). (*) under the spectral resolution. N.O. = not observed.

	νO-H	**Δ(νO-H)**	**νC=O**	**Δ(νC=O)**	**νN-H**	**Δ(νN-H)**
CAT-H	3443, 3321	—	—	—	—	—
CAT	3444, 3320	—	—	—	—	—
TEO	—	—	1705, 1662	—	3120	—
TEO-H	3360	—	1708, 1695, 1642	3, −10, −20	3131	11
CAT-TEO-H	3517, 3454	73, 314	1699, 1666, 1629	−6, 4, −33	N.O.	—
CAT-TEO	3151	−293, −169	1714, 1704, 1633	9, −1 *, −29	N.O.	—
CAT-TEO-MIX	3345, 3324	—	1705, 1662	—	3120	—

The carbonyl C=O stretching bands of TEO (Figure 2) were shifted in the IR spectrum of the CAT-TEO ground mixture as a consequence of the formation of the cocrystal (Table 1), with absolute values of Δ(νC=O) less than 20 cm^{-1}. This shift is in accordance with the formation of the neutral C=O···H-O hydrogen bond interaction, discarding the proton transfer [16].

The solid form of TEO presents polymorphism, and each polymorph gives a different vibrational spectrum [26]. On the other hand, there are not any reports about polymorphs of CAT. To discard polymorphic transitions as a consequence of the grinding, CAT and TEO were ground individually with dichloromethane. After 15 min of grinding, the IR spectra were similar to those obtained before grinding, which discards polymorphic transformations (Figure S1 of supplementary material) as a consequence of the grinding.

Possible effects of water absorption from the air during mechanochemical grinding over the starting products and the mixtures were evaluated by grinding CAT and TEO with water (CAT-H and TEO-H, Figure 2); the CAT-TEO mixture was ground with water (CAT-TEO-H, Figure 2). The IR spectrum of TEO ground with water, recorded after 15 min of grinding (TEO-H, Figure 2), was different with respect to the anhydrous form (TEO, Figure 2), showing shifts in the N-H, C=O and C-H(alkyl) stretching frequencies, and the appearance of the broad O-H band in the range of the 3350 to 3360 cm^{-1}. The spectrum (TEO-H, Figure 2) is similar to that reported for the TEO hydrate [18]. Two characteristic bands in the IR spectrum of TEO-H are the N-H stretching frequency at 3139 cm^{-1} and the C-H alkyl stretching frequency at 3106 cm^{-1}.

Contrarily to TEO, the IR frequencies of CAT ground with water (CAT-H, Figure 2) did not show any significant shift with respect to the anhydrous form. The O-H band of the water appeared to overlap with the O-H bands of CAT. It is noteworthy that after the grinding of CAT-H, a liquid product (catechol solution) was obtained, so the IR spectrum of CAT-H was obtained in liquid form. The fact that water acts as an interference in the IR spectrum of CAT-H means that it is not part of the crystalline lattice of the solid, discarding the hydration. This is in agreement with the absence of reports of hydrated solid forms of CAT.

The IR spectrum of the CAT-TEO 1:1 mixture ground with water (CAT-TEO-H, Figure 2) showed a different pattern with respect to the anhydrous ground mixture (CAT-TEO, Figure 2). The IR spectrum of CAT-TEO-H showed two O-H bands at 3517 and 3454 cm^{-1}; meanwhile, CAT-TEO showed a single O-H band at 3151 cm^{-1}. In the same way, the IR spectrum of CAT-TEO-H showed a different pattern of C=O bands with respect to the CAT-TEO spectrum. This allows determining that the CAT-TEO-H ground solid is the cocrystal hydrate.

3.2. Powder X-ray Diffraction

In order to confirm the formation of a new solid phase belonging to the CAT-TEO cocrystal, powder X-ray diffraction studies (PXRD) were performed. The PXRD pattern of CAT-TEO ground with dichloromethane after 15 min of grinding time was different to

the starting solids CAT and TEO, and also to the hydrated CAT-TEO-H ground mixture (Figure 3). The PXRD pattern of TEO-H is similar to that reported for the theophylline hydrate [18]. The absence of the signals of CAT at low 2θ in the XRPD diffractograms of the anhydrous CAT-TEO ground mixture suggests the complete conversion of CAT and TEO into the CAT-TEO cocrystal. The PXRD patterns of CAT-TEO showed characteristic peaks at 2θ = 9.0° 10.5°, 13.1°, 14.7°, 15.8° 16.5°, 17.6°, 20.3°, 22.9°, 26.3°, 29.0°.

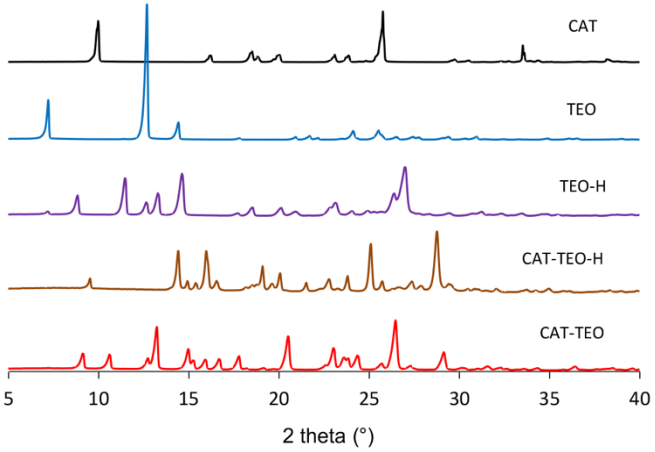

Figure 3. X-ray diffractograms showing the formation of a new solid phase belonging to CAT-TEO cocrystal. CAT (catechol); TEO (theophylline); TEO-H (theophylline ground with water); CAT-TEO-H (catechol and theophylline ground with water); CAT-TEO (catechol and theophylline ground with dichloromethane).

3.3. Thermal Analysis

Differential scanning calorimetry (DSC) and thermogravimetric analysis (TGA) experiments were carried out to study the thermal behavior of the CAT-TEO cocrystal. DSC results revealed that the melting point of the CAT-TEO cocrystal (134.16 °C) was different from CAT (100 to 103 °C) [27] and TEO (270 to 274 °C) [28], indicating the formation of a new crystalline solid phase. Meanwhile, the TGA curve of the CAT-TEO cocrystal indicates the absence of hydration (DSC and TGA curves are shown in Figure S2 of supplementary material).

3.4. Solid-State ^{13}C NMR

Solid-state ^{13}C nuclear magnetic resonance spectra of CAT, TEO and the CAT-TEO cocrystal (Figure 4) were obtained to acquire information about hydrogen bonding interactions and crystallography. The ^{13}C NMR chemical shifts of the CAT and TEO starting products were assigned according to previous reports [8,29]. The ^{13}C NMR spectrum of free CAT showed the half of total signals due to the C2 symmetry.

Most of the ^{13}C NMR signals in the spectrum of the CAT-TEO cocrystal were shifted with respect to the starting CAT and TEO (Table 2); this is due to the change of the chemical environment as a consequence of the cocrystal formation. Carbonyl carbons of TEO are sensitive to hydrogen bonding formation. The carbonyl C2 signal of TEO was shifted in the CAT-TEO cocrystal with respect to the free TEO ($\Delta\delta$ ^{13}C = 3.6 ppm), due to the formation of the C=O···H-O hydrogen bond interaction. The C5 signal was sensitive to the change of chemical environment with $\Delta\delta$ ^{13}C = −3 ppm. C6 and C7 also showed significant shifts C6 $\Delta\delta$ ^{13}C = −2.4 ppm, and C7 $\Delta\delta$ ^{13}C = 1.9 ppm.

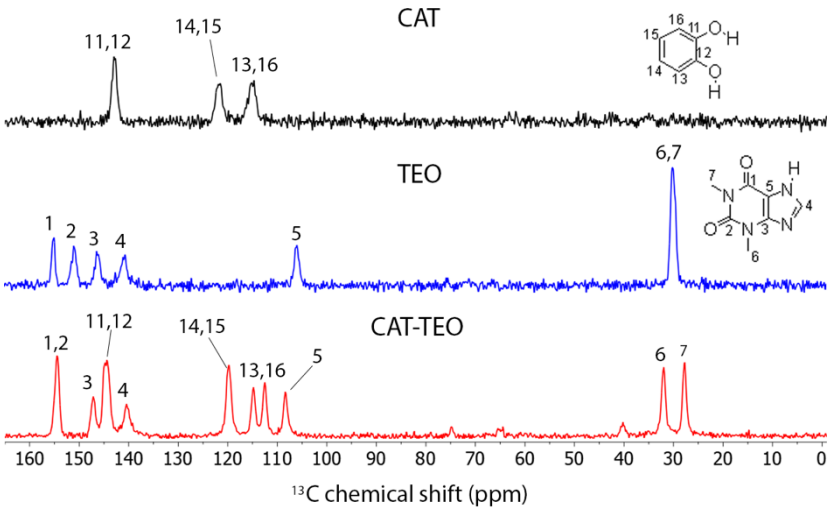

Figure 4. Solid-state ^{13}C CP/MAS NMR spectra (δ = ppm) of the CAT-TEO cocrystal and the starting products catechol (CAT) and theophylline (TEO).

Table 2. CP/MAS solid state ^{13}C NMR chemical shifts of CAT, TEO and the CAT-TEO cocrystal.

	C1	**C2**	**C3**	**C4**	**C5**	**C6**	**C7**
TEO	154.9	150.9	146.3	140.5	105.8	30.0	30.0
CAT-TEO	154.5	154.5	144.2	140.2	108.3	31.9	27.6
	C11	**C12**	**C13**	**C14**	**C15**	**C16**	
CAT	142.9	142.9	114.6	121.5	121.5	114.6	
CAT-TEO	144.7	144.7	114.7 112.4	119.8	119.8	114.7 112.4	

All the ^{13}C NMR signals of CAT in the CAT-TEO spectrum were shifted with respect to free CAT as a consequence of the formation of the cocrystal (Table 2). The C13 and C16 signals appeared to be split, indicating an asymmetric chemical environment in these carbons.

3.5. Theoretical Calculations

To validate the information obtained from the ^{13}C CP/MAS NMR study (δexp), the gauge including the atomic orbital (GIAO) method at a B3LYP/6-31G(d,p) level of theory was used to calculate the isotropic magnetic shielding (σiso) and predict the ^{13}C NMR chemical shifts (δcalc) of the CAT-TEO$_1$ and CAT-TEO$_2$ models (Table 3, Figure 5). The calculated chemical shifts are in agreement with the experimental results because the correlation coefficient R^2 (Figure S3 supplementary material) is 0.997 and 0.996, respectively.

Density functional theory methods (DFT) allow the calculation of molecular properties of the molecular complexes. One of these properties is the optimization of the geometry in the gas phase, which gives an idea about the molecular structure of a complex [30,31]. In the same way, natural bond orbital (NBO) analysis gives information about the electron density distribution involved in the formation of hydrogen bonds among the molecules of the complexes [32,33].

Table 3. Calculated (δcalc) and experimental (δexp) CP/MAS solid state ^{13}C NMR chemical shifts (ppm) of TEO and CAT in the 1:1 anhydrous ground mixture, and calculated (root mean square error less than 4.0) GIAO isotropic magnetic shielding tensors (σiso).

	C1	**C2**	**C3**	**C4**	**C5**	**C6**	**C7**
CAT-TEO (δ_{exp})	154.5	154.5	144.2	140.2	108.3	31.9	27.6
CAT-TEO$_1$ (δ_{calc})	154.6	155.3	150.2	138.2	114.0	38.9	35.7
σ_{iso}	(45.3)	(44.6)	(49.7)	(61.7)	(85.9)	(161.0)	(164.1)
CAT-TEO$_2$ (δ_{calc})	157.5	151.9	151.9	139.7	113.4	37.2	36.7
σ_{iso}	(42.4)	(48.0)	(48.0)	(60.2)	(86.5)	(162.7)	(163.1)
	C11	**C12**	**C13**	**C14**	**C15**	**C16**	
CAT-TEO (δ_{exp})	144.7	144.7	114.7 112.4	119.8	119.8	114.7 112.4	
CAT-TEO$_1$ (δ_{calc})	148.8	147	116	121.3	122.9	117.4	
σ_{iso}	(51.1)	(52.9)	(83.9)	(78.6)	(77.0)	(82.4)	
CAT-TEO$_2$ (δ_{calc})	146.6	146.5	116.7	122.8	122.9	119.3	
σ_{iso}	(53.3)	(53.4)	(83.2)	(77.1)	(76.0)	(80.5)	

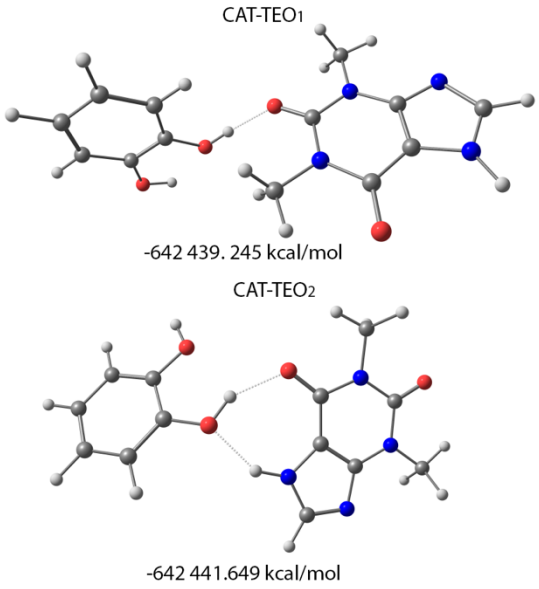

Figure 5. Possible C=O···H-O hydrogen bond models and optimized structures of the CAT-TEO cocrystal.

In order to obtain structural information about the intermolecular hydrogen bond patterns involved in the formation of the CAT-TEO cocrystal, DFT calculations at B3LYP/6-31G(d,p) level of theory were performed in CAT-TEO$_1$ and CAT-TEO$_2$ models (Figure 5) considering the two possible C=O···H-O hydrogen bond patterns in the CAT-TEO cocrystal. The CAT-TEO$_2$ model is the most stable structure (by only 2.404 kcal/mol) involving the C=O(2)···H-O(11) and the N-H···O(11) hydrogen bond interactions (Figure 5); meanwhile, the CAT-TEO$_1$ model is in accordance with the ^{13}C NMR shifts because the carbonyl C2 signal showed a $\Delta\delta$ ^{13}C = 3.6 ppm in the CAT-TEO cocrystal with respect to the free TEO. This deshielding suggests the formation of the C=O···H-O hydrogen bonding in this position, contrary to the carbonyl C1, which showed a $\Delta\delta$ ^{13}C = −0.4 ppm. This is also in accordance with previous reports about synthon hierarchies in cocrystals of TEO with hydroxybenzoic acids with respect to the hydrogen bonds involving phenolic O-H groups, in which the O-H···O=C(urea) interaction is preferred over the O-H···O=C(amide) interaction because the O=C(amide) is involved in the dimerization of TEO by the N-H···O=C(amide) hydrogen bond synthon [5].

The C=O···H-O hydrogen bond interaction in the CAT-TEO$_2$ model is formed by the overlap of the lone pair electrons of the carbonylic oxygen (nO) with the σ*(H–O) anti-bonding orbital (the energetic parameters are shown in Table S1 of supplementary material). The superficial analysis at DFT-B3LYP/6-31G(d,p) confirmed the preference for the C=O(2)···H-O in the CAT-TEO$_2$ model cocrystal (Figure 6), as suggested by the ^{13}C NMR results because in the spectra the C2 carbon showed a higher shift with respect to the C1. The hydrogen bond distances are similar to the reported for cocrystals of dihydroxybenzenes [15,24].

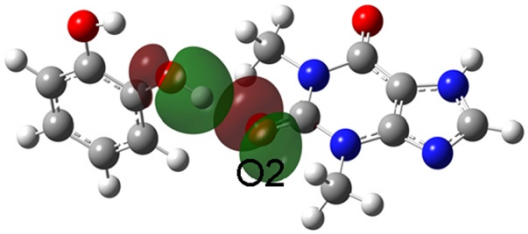

Figure 6. Natural bonding orbital interactions of the CAT-TEO$_1$ model cocrystal.

4. Conclusions

The CAT-TEO cocrystal was prepared by the solvent-assisted grinding method and characterized by infrared spectroscopy, powder X-ray diffraction and solid-state CP/MAS ^{13}C NMR. The infrared spectroscopy study allowed to determine that the formation of the cocrystal, directed by C=O···H-O hydrogen bond interactions and confirmed by ^{13}C solid-state NMR and theoretical calculations. Hydration of the CAT-TEO cocrystal was discarded because the IR spectrum of the anhydrous CAT-TEO mixture was different with respect to the hydrated ground mixture (CAT-TEO-H), and the TGA curve does not show hydration. IR spectroscopy allowed to determine the hydration of theophylline (TEO-H) and the CAT-TEO cocrystal (CAT-TEO-H) as a consequence of the grinding with water. The formation of the solid phase belonging to the CAT-TEO cocrystal was confirmed by powder X-ray diffraction. Thermal analysis revealed that the melting point of the CAT-TEO cocrystal is different from the starting compounds. The GIAO ^{13}C NMR chemical shift values were correlated with the experimental data.

Supplementary Materials: The following are available online at https://www.mdpi.com/article/10.3390/app11093810/s1, Figure S1: Figure S1. IR spectra of (a) bulk catechol; (b) catechol ground with dichloromethane after 15 min of grinding; c) bulk theophylline; d) theophylline ground with dichloromethane after 15 min of grinding; Figure S2: DSC and TGA curves of the CAT-TEO cocrystal; Figure S3: Correlations of the experimental and theoretical shielding parameters for CAT-TEO$_1$ and CAT-TEO$_2$ models. Table S1: Theoretical optimization energy and second order perturbation theory analysis of Fock matrix in NBO basis of the optimized CAT-TEO models.

Author Contributions: Conceptualization, J.S.G.-G.; methodology, R.J.-L.; software, D.O.-R.; formal analysis, G.G.-C.; F.J.M.-M.; writing—original draft preparation, J.S.G.-G.; writing—review and editing, J.S.G.-G.; F.J.M.-M.; D.O.-R. All authors have read and agreed to the published version of the manuscript.

Funding: This research was funded by Universidad de la Cañada PFI 12/15.

Institutional Review Board Statement: Not applicable.

Informed Consent Statement: Not applicable.

Data Availability Statement: Not applicable.

Conflicts of Interest: The authors declare no conflict of interest.

References

1. Barnes, P.J. Theophylline. *Am. J. Respir. Crit. Care. Med.* **2013**, *188*, 901–906. [CrossRef]
2. Dutta, A.; Roy, N.; Das, K.; Roy, D.; Ghosh, R.; Roy, M.N. Synthesis and Characterization of Host Guest Inclusion Complexes of Cyclodextrin Molecules with Theophylline by Diverse Methodologies. *Emerg. Sci. J.* **2020**, *4*, 52–72. [CrossRef]
3. Francesconi, O.; Ienco, A.; Nativi, C.; Roelens, S. Effective Recognition of Caffeine by Diaminocarbazolic Receptors. *ChemPlusChem* **2020**, *85*, 1369–1373. [CrossRef]
4. Jayram, P.; Sudheer, P. Pharmaceutical Co-crystals: A Systematic Review. *Int. J. Pharm. Investig.* **2020**, *10*, 246–252. [CrossRef]
5. Bucar, D.K.; Henry, R.F.; Zhang, G.G.Z.; MacGillivray, L.R. Synthon Hierarchies in Crystal Forms Composed of Theophylline and Hydroxybenzoic Acids: Cocrystal Screening via Solution-Mediated Phase Transformation. *Cryst. Growth Des.* **2014**, *14*, 5318–5328. [CrossRef]
6. Heiden, S.; Tröbs, L.; Wenzel, K.; Emmerling, F. Mechanochemical synthesis and structural characterisation of a theophylline-benzoic acid cocrystal (1:1). *CrystEngComm* **2012**, *14*, 5128–5129. [CrossRef]
7. Surov, A.O.; Voronin, A.P.; Manin, A.N.; Manin, N.G.; Kuzmina, L.G.; Churakov, A.V.; Perlovich, G.L. Pharmaceutical Cocrystals of Diflunisal and Diclofenac with Theophylline. *Mol. Pharm.* **2014**, *11*, 3707–3715. [CrossRef]
8. Li, P.; Chu, Y.; Wang, L.; Wenslow, R.M., Jr.; Yu, K.; Zhang, H.; Denga, Z. Structure determination of the theophylline–nicotinamide cocrystal: A combined powder XRD, 1D solid-state NMR, and theoretical calculation study. *CrystEngComm* **2014**, *16*, 3141–3147. [CrossRef]
9. Wang, L.; Luo, M.; Li, J.; Wang, J.; Zhang, H.; Deng, Z. Sweet Theophylline Cocrystal with Two Tautomers of Acesulfame. *Cryst. Growth Des.* **2015**, *15*, 2574–2578. [CrossRef]
10. Gangavaram, S.; Raghavender, S.; Sanphui, P.; Pal, S.; Manjunatha, S.G.; Nambiar, S.; Nangia, A. Polymorphs and cocrystals of nalidixic acid. *Cryst. Growth Des.* **2012**, *12*, 4963–4971. [CrossRef]
11. Bolla, G.; Sanphui, P.; Nangia, A. Solubility advantage of tenoxicam phenolic cocrystals compared to salts. *Cryst. Growth Des.* **2013**, *13*, 1988–2003. [CrossRef]
12. Arabiani, M.R.; Bhunia, S.; Teja, P.K.; Lodagekar, A.; Chavan, R.B.; Shastri, N.R.; Reddi, C.M.; Shelat, P.; Dave, D. Brexpiprazole–catechol cocrystal: Structure elucidation, excipient compatibility and stability. *CrystEngComm* **2019**, *21*, 6703–6708. [CrossRef]
13. González-González, J.S.; Martínez-Santiago, A.M.M.; Martínez-Martínez, F.J.; Emparán-Legaspi, M.J.; Pineda-Contreras, A.; Flores-Alamo, M.; García-Ortega, H. Cocrystals of Isoniazid with Polyphenols: Mechanochemical Synthesis and Molecular Structure. *Crystals* **2020**, *10*, 569. [CrossRef]
14. Rodrigues, M.; Baptista, B.; Almeida, J.L.; Cruz, S.M. Pharmaceutical cocrystallization techniques. Advances and challenges. *Int. J. Pharm.* **2018**, *547*, 404–420. [CrossRef]
15. Izutsu, K.; Koide, T.; Takata, N.; Ikeda, Y.; Ono, M.; Inoue, M.; Fukami, T.; Yonemochi, E. Characterization and Quality Control of Pharmaceutical Cocrystals. *Chem. Pharm. Bull.* **2016**, *64*, 1421–1430. [CrossRef] [PubMed]
16. Childs, S.L.; Stahly, G.P.; Park, A. The Salt-Cocrystal Continuum: The Influence of Crystal Structure on Ionization State. *Mol. Pharm.* **2007**, *4*, 323–338. [CrossRef]
17. Chan, K.L.A.; Fleming, O.S.; Kazarian, S.G.; Vassou, D.; Chryssikos, G.D.; Gionis, V. Polymorphism and devitrification of nifedipine under controlled humidity: A combined FT-Raman, IR and Raman microscopic investigation. *J. Raman Spectrosc.* **2004**, *35*, 353–359. [CrossRef]
18. González-González, J.S.; Zúñiga-Lemus, O.; Hernández-Galindo, M.C. Hydrated Solid Forms of Theophylline and Caffeine Obtained by Mechanochemistry. *IOSR J. Pharm.* **2017**, *7*, 28–30. [CrossRef]
19. Grdadolnik, J. ATR-FTIR Spectroscopy: Its Advantages and Limitations. *Acta Chim. Slov.* **2002**, *49*, 631–642.
20. Mukherjee, A.; Tothadi, S.; Chakraborty, S.; Ganguly, S.; Desiraju, G.R. Synthon identification in co-crystals and polymorphs with IR spectroscopy. Primary amides as a case study. *CrystEngComm* **2013**, *15*, 4640–4654. [CrossRef]
21. Vogt, F.G.; Clawson, J.S.; Strohmeier, M.; Edwards, A.J.; Pham, T.N.; Watson, S.A. Solid-state NMR analysis of organic cocrystals and complexes. *Cryst. Growth Des.* **2009**, *9*, 921–937. [CrossRef]
22. Li, M.; Xu, W.; Su, Y. Solid-state NMR spectroscopy in pharmaceutical sciences. *Trends Anal. Chem.* **2021**, *135*, 116152. [CrossRef]
23. Frisch, M.J.; Trucks, G.W.; Schlegel, H.B.; Scuseria, G.E.; Robb, M.A.; Cheeseman, J.R.; Scalmani, G.; Barone, V.; Petersson, G.A.; Nakatsuji, H.; et al. *Gaussian 16, Revision C.01*; Gaussian, Inc.: Wallingford, CT, USA, 2016.
24. González-González, J.S.; Martínez-Martínez, F.J.; García-Báez, E.V.; Cruz, A.; Morín-Sánchez, L.M.; Rojas-Lima, S.; Padilla-Martínez, I.I. Molecular complexes of diethyl N, N′-1, 3-phenyldioxalamate and resorcinols: Conformational switching through intramolecular three-centered hydrogen-bonding. *Cryst. Growth Des.* **2014**, *14*, 628–642. [CrossRef]
25. Saucedo-Balderas, M.M.; Delgado-Alfaro, R.A.; Martínez-Martínez, F.J.; Ortegón-Reyna, D.; Bernabé-Pineda, M.; Zúñiga-Lemus, O.; González-González, J.S. Synthesis, Molecular Structure of Diethyl Phenylenebis (Methylene) Dicarbamates and FTIR Spectroscopy Molecular Recognition Study with Benzenediols. *J. Braz. Chem. Soc.* **2015**, *26*, 396–402. [CrossRef]
26. Seton, L.; Khamar, D.; Bradshaw, I.J.; Hutcheon, G.A. Solid state forms of theophylline: Presenting a new anhydrous polymorph. *Cryst. Growth Des.* **2010**, *10*, 3879–3886. [CrossRef]
27. 1,2-Dihydroxybenzene. Available online: https://www.sigmaaldrich.com/catalog/product/sial/135011?lang=es&region=MX&cm_sp=Insite-_-caSrpResults_srpRecs_srpModel_catechol-_-srpRecs3-1 (accessed on 27 February 2021).
28. Theophylline. Available online: https://www.sigmaaldrich.com/catalog/product/sigma/t1633?lang=es&region=MX (accessed on 27 February 2021).

29. Finkelstein-Shapiro, D.; Davidowski, S.K.; Lee, P.B.; Guo, C.; Holland, G.P.; Rajh, T.; Kimberly, A.; Gray, K.A.; Yarger, J.L.; Calatayud, M. Direct evidence of chelated geometry of catechol on TiO2 by a combined solid-state NMR and DFT study. *J. Phys. Chem. C* **2016**, *120*, 23625–23630. [CrossRef]
30. Du, Y.; Fang, X.; Zhang, Q.; Zhang, H.L.; Hong, Z. Spectroscopic investigation on cocrystal formation between adenine and fumaric acid based on infrared and Raman techniques. *Spectrochim. Acta Part A Mol. Biomol. Spectrosc.* **2016**, *153*, 580–585. [CrossRef]
31. Bruni, G.; Maietta, M.; Berbenni, V.; Mustarelli, P.; Ferrara, C.; Freccero, M.; Grande, V.; Maggi, L.; Milanese, C.; Girella, A.; et al. Mechanochemical Synthesis of Bumetanide-4-Aminobenzoic Acid Molecular Cocrystals: A Facile and Green Approach to Drug Optimization. *J. Phys. Chem. B* **2014**, *118*, 9180–9190. [CrossRef]
32. Srivastava, K.; Shimpi, M.R.; Srivastava, A.; Tandon, P.; Sinha, K.; Velaga, S.P. Vibrational analysis and chemical activity of paracetamol–oxalic acid cocrystal based on monomer and dimer calculations: DFT and AIM approach. *RSC Adv.* **2016**, *6*, 10024–10037. [CrossRef]
33. Majerz, I. Directionality of Inter- and Intramolecular OHO Hydrogen Bonds: DFT Study Followed by AIM and NBO Analysis. *J. Phys. Chem. A* **2012**, *116*, 7992–8000. [CrossRef]